

Electronic structure of $\text{Li}_{1+x}[\text{Mn}_{0.5}\text{Ni}_{0.5}]_{1-x}\text{O}_2$ studied by photoemission and x-ray absorption spectroscopy

Y. Yokoyama,^{1,2} D. Ootsuki,¹ T. Sugimoto,³ H. Wadati,²
J. Okabayashi,⁴ Xu Yang,⁵ Fei Du,⁵ Gang Chen,⁵ and T. Mizokawa⁶

¹*Department of Physics, University of Tokyo, Chiba 277-8561, Japan*

²*Institute for Solid State Physics, University of Tokyo, Chiba 277-8581, Japan*

³*Department of Complexity Science and Engineering, University of Tokyo, Chiba 277-8561, Japan*

⁴*Research Center for Spectrochemistry, University of Tokyo, Tokyo 113-0033, Japan*

⁵*Key Laboratory of Physics and Technology for Advanced Batteries (Ministry of Education),
College of physics, Jilin University, Changchun 130012, People's Republic of China*

⁶*Department of Applied Physics, Waseda University, Tokyo 169-8555, Japan*

(Dated: August 24, 2018)

We have studied the electronic structure of $\text{Li}_{1+x}[\text{Mn}_{0.5}\text{Ni}_{0.5}]_{1-x}\text{O}_2$ ($x = 0.00$ and 0.05), one of the promising cathode materials for Li ion battery, by means of x-ray photoemission and absorption spectroscopy. The results show that the valences of Mn and Ni are basically $4+$ and $2+$, respectively. However, the Mn^{3+} component in the $x = 0.00$ sample gradually increases with the bulk sensitivity of the experiment, indicating that the Jahn-Teller active Mn^{3+} ions are introduced in the bulk due to the site exchange between Li and Ni. The Mn^{3+} component gets negligibly small in the $x = 0.05$ sample, which indicates that the excess Li suppresses the site exchange and removes the Jahn-Teller active Mn^{3+} .

PACS numbers: 71.28.+d, 79.60.-i

Layered transition-metal oxides, in which transition-metal M atoms form two-dimensional triangular lattices with edge-sharing MO_6 octahedra, are known as cathode materials for rechargeable batteries. In particular, Li_xCoO_2 has been widely studied for the practical use as a positive electrode material in commercial Li ion batteries [1]. Rechargeable batteries using Li_xCoO_2 cathodes exhibit the highest performance among batteries using similar transition metal oxides [1–4]. However, Co is relatively expensive and alternative cathode materials should be developed with less expensive transition-metal elements. Since Mn and Ni are less expensive than Co, $\text{LiMn}_{0.5}\text{Ni}_{0.5}\text{O}_2$ is one of the promising materials [5, 6]. $\text{LiMn}_{0.5}\text{Ni}_{0.5}\text{O}_2$ has the layered $\alpha\text{-NaFeO}_2$ structure (rhombohedral system, space group $R\bar{3}m$), and consists of the MO_2 ($M = \text{Mn}$ and Ni) layers and the interlayers of Li ions. The Li ions occupy the octahedral sites between the MO_2 layers. In the charging process, Ni^{2+} ejects two electrons and changes to Ni^{4+} . By increasing the ratio of Li in $\text{Li}_{1+x}[\text{Mn}_{0.5}\text{Ni}_{0.5}]_{1-x}\text{O}_2$, the capacity retention is improved as x increases up to 0.05 [7]. If Jahn-Teller active Mn^{3+} species exist, the capacity retention would be degraded due to the Jahn-Teller distortion of Mn^{3+}O_6 octahedron. Moreover, the exchange between the Ni^{2+} and Li^+ ions plays important roles [7]. In order to clarify the effect of the excess Li ions on the electronic structure, we have performed x-ray photoemission spectroscopy (XPS) and x-ray absorption spectroscopy (XAS) measurements of $\text{Li}_{1+x}[\text{Mn}_{0.5}\text{Ni}_{0.5}]_{1-x}\text{O}_2$.

Powder samples of $\text{Li}_{1+x}[\text{Mn}_{0.5}\text{Ni}_{0.5}]_{1-x}\text{O}_2$ ($x = 0.00$ and 0.05) were grown by solid state reaction. The samples were pressed onto the carbon tapes which were attached to the sample holder, and were introduced to the chambers under the ultrahigh vacuum. XPS measure-

ments were performed by using JEOL JPS-9200 with a Mg $K\alpha$ x-ray source (1253.6 eV). XAS measurements were performed at beamline 7A, Photon Factory, KEK. In the total electron yield (TEY) mode, the total electrons were counted by measuring the sample current. In the fluorescence yield (FY) mode, the O $1s$ x-ray emission was measured for the inverse partial fluorescence yield (IPFY) method [8, 9].

Figures 1(a) and (b) show the Ni $2p$ and Mn $2p$ XPS spectra of $\text{Li}_{1+x}[\text{Mn}_{0.5}\text{Ni}_{0.5}]_{1-x}\text{O}_2$ ($x = 0.00$ and 0.05). In the Ni $2p$ XPS, the peak around 860 eV corresponds to Ni $2p_{3/2}$ and the peak around 880 eV corresponds to Ni $2p_{1/2}$. In the Mn $2p$ XPS, the peaks around 643 eV and 655 eV correspond to the Mn $2p_{3/2}$ and Mn $2p_{1/2}$ branches, respectively. The peak shift with x is not observed in the Mn $2p$ and Ni $2p$ core levels, showing that the valences of Mn and Ni do not depend on x appreciably.

In Fig. 2, the Ni $2p$ XPS is compared with the configuration interaction (CI) calculation on a NiO_6 cluster model with $\Delta = 4.5$ eV, $(pd\sigma) = -1.5$ eV, and $U = 7.0$ eV. In the present cluster model, the ground state with ${}^3A_{2g}$ symmetry is given by the linear combination of d^8 , d^9L , and $d^{10}L^2$ configurations, where L denotes an O $2p$ hole. The energy difference between d^8 and d^9L corresponds to Δ and that between d^9L and $d^{10}L^2$ is basically given by $\Delta + U$. The final states are described by the linear combinations of cd^8 , cd^9L , and $cd^{10}L^2$ configurations, where c denotes an Ni $2p$ hole. The Coulomb interaction between the Ni $3d$ electrons are given by the Slater integrals $F^0(3d, 3d)$, $F^2(3d, 3d)$, and $F^4(3d, 3d)$. The average Ni $3d$ -Ni $3d$ Coulomb interaction U is expressed by $F^0(3d, 3d)$ and is an adjustable parameter. $F^2(3d, 3d)$ and $F^4(3d, 3d)$ are fixed to 80% of the atomic

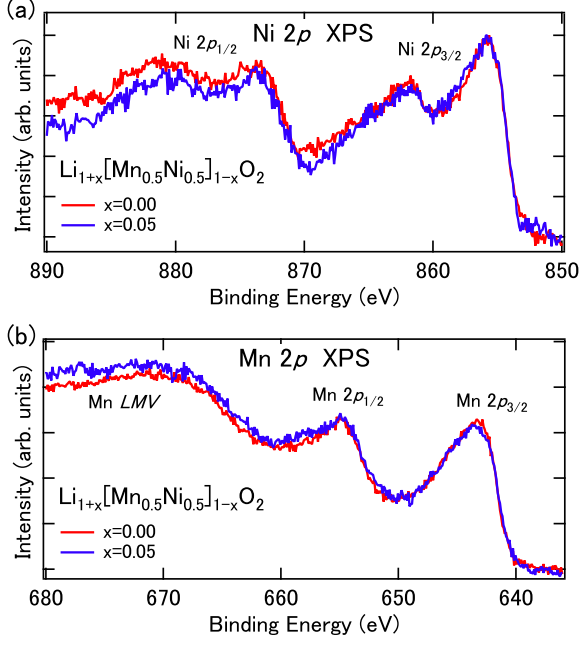


FIG. 1: (a) Ni 2p and (b) Mn 2p XPS of $\text{Li}_{1+x}[\text{Mn}_{0.5}\text{Ni}_{0.5}]_{1-x}\text{O}_2$ ($x = 0.00$ and 0.05).

Hartree-Fock values [10]. The Coulomb interaction between the Ni 2p core hole and the Ni 3d electron is expressed by the Slater integrals $F^0(2p,3d)$, $F^2(2p,3d)$, and $G^1(2p,3d)$. The average Ni 2p-Ni 3d Coulomb interaction Q is expressed by $F^0(2p,3d)$ and is fixed to $U/0.8$. $F^2(2p,3d)$ and $G^1(2p,3d)$ are fixed to 80% of the atomic Hartree-Fock values [10]. The energy difference between cd^8 and cd^9L corresponds to $\Delta - Q$ and that between cd^9L and $cd^{10}L^2$ is $\Delta - Q + U$. The transfer integrals between the Ni 3d and O 2p orbitals are given by $(pd\sigma)$ and $(pd\pi)$ where the ratio $(pd\sigma)/(pd\pi)$ is fixed at -2.16. As shown in Fig. 2, the charge-transfer satellite is well reproduced by the calculation. The obtained parameters satisfy $\Delta < U$, indicating that the Ni^{2+} state falls in the charge-transfer regime. Since $\Delta - Q$ is negative, the main and satellite peaks are dominated by the cd^9L and cd^8 configurations, respectively.

We performed XAS measurements with various x in the TEY mode. The probing depth of the TEY XAS measurement is larger than that of the XPS measurement. Figure 3(a) and (b) show the Ni 2p TEY XAS spectra and their comparison with the reference data [11]. The peak around 850 eV corresponds to the Ni $2p_{3/2}$ edge and the peak around 867 eV corresponds to the Ni $2p_{1/2}$ edge. The lineshape shows that the valence of Ni is dominated by 2+ and does not change as the ratio of Li increases.

In the Mn 2p XAS shown in Fig. 3(c), the peak around 640 eV corresponds to the transition from the Mn $2p_{3/2}$ core level to the Mn 3d e_g state and the peak around 643 eV corresponds to the transition from the Mn $2p_{3/2}$

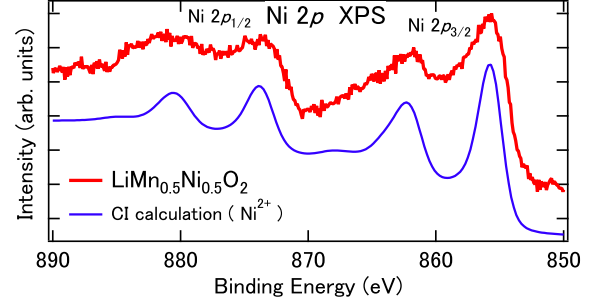


FIG. 2: Calculated Ni 2p XPS spectrum (blue line) compared with the Ni 2p XPS of $\text{LiMn}_{0.5}\text{Ni}_{0.5}\text{O}_2$ (red line).

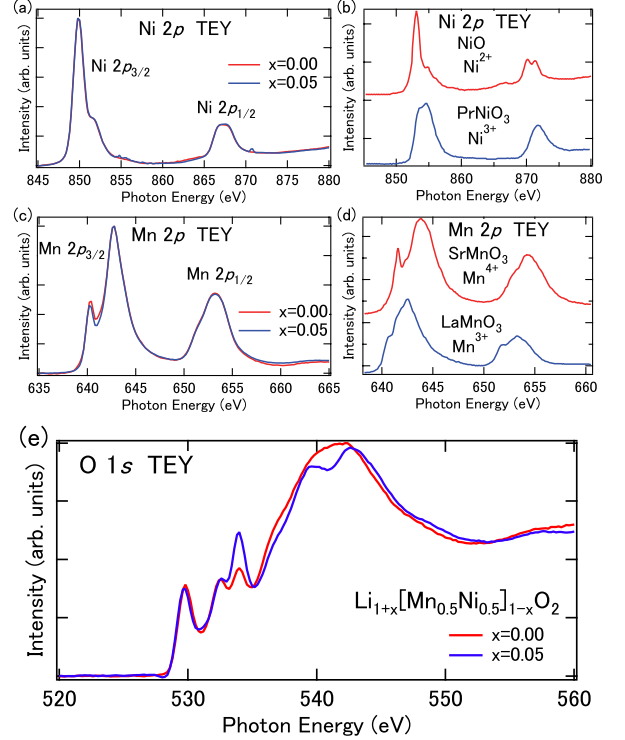


FIG. 3: (a) Ni 2p XAS spectra of $\text{Li}_{1+x}[\text{Mn}_{0.5}\text{Ni}_{0.5}]_{1-x}\text{O}_2$ ($x = 0.00$ and 0.05) and (b) their comparison with the reference data [11]. (c) Mn 2p XAS spectra of $\text{Li}_{1+x}[\text{Mn}_{0.5}\text{Ni}_{0.5}]_{1-x}\text{O}_2$ and (d) their comparison with the reference data [12]. (e) O 1s XAS spectra of $\text{Li}_{1+x}[\text{Mn}_{0.5}\text{Ni}_{0.5}]_{1-x}\text{O}_2$.

core level to the Mn 3d t_{2g} state. The other peak around 653 eV corresponds to the Mn $2p_{1/2}$ edge. The lineshape indicates that the valence of Mn is almost 4+. However, it is observed that the height of the e_g edge relative to the t_{2g} edge gets slightly lower as the ratio of Li increases. Considering the fact that the Ni 2p spectral change is negligible, the Mn 2p spectral change with x should be taken into account seriously.

Figure 3(e) shows the O 1s TEY XAS spectra that represent the transitions from the O 1s core level to the

O $2p$ orbitals mixed into the unoccupied Mn and Ni $3d$ states. Interestingly, the peak around 533 eV gains its intensity with x and would be related to the Mn valence change observed in the Mn $2p$ XAS.

Figure 4(a) shows the Ni $2p$ TEY XAS spectrum and its comparison with the CI calculation. By using the parameters obtained in Fig. 2, we calculated the theoretical spectrum and attempted to reproduce the experimental result. The theoretical spectrum (calculated by $\Delta = 4.5$ eV, $pd\sigma = -1.5$ eV, and $U = 7.0$ eV) is in good agreement with the experimental spectrum, indicating that the Ni $2p$ TEY XAS spectra are consistent with the Ni $2p$ XPS spectra. In the Ni $2p$ XAS, the final states are described by the linear combinations of cd^9 and $cd^{10}L$ configurations. Since $\Delta - Q + U$ is positive, the main peak is dominated by the cd^9 configurations and the satellite peak is very small. In this sense, the charge transferred configurations are irrelevant in the case of Ni $2p$ XAS.

Figure 4(b) shows the Mn $2p$ TEY XAS spectrum and its comparison with the calculated spectra for the transitions from d^3 to cd^4 . Since $\Delta - Q + U$ is positive and the charge transfer satellite is not observed, the Mn $2p$ XAS lineshape can be evaluated without including the charge transferred configurations. Instead of the O $2p$ -Mn $3d$ transfer integrals, the energy splitting between the e_g and t_{2g} orbitals ($10Dq$) is adjusted to reproduce the experimental result. The estimated value of $10Dq$ is 2.0 or 2.5 eV as shown in Fig. 4(b). By using $10Dq = 2.5$ eV, we calculated the Mn^{3+} spectrum for the transitions from d^4 to cd^5 . Then, we added the spectrum of Mn^{3+} to that of Mn^{4+} , trying to reproduce the experimental spectra of $Li_{1+x}[Mn_{0.5}Ni_{0.5}]_{1-x}O_2$ ($x = 0.00$ and 0.05). Figure 4(c) shows the Mn $2p$ XAS spectra and their comparison with the theoretical spectra which correspond to the mixed valence of Mn^{4+} and Mn^{3+} . In the experimental result, the intensity of e_g peak (~ 640.2 eV) relative to that of t_{2g} peak (~ 642.7 eV) is reduced with x . The theoretical spectra indicate that the intensity of e_g peak (~ 640.5 eV) relative to that of t_{2g} peak (~ 642.5 eV) gets stronger as the ratio of Mn^{3+} increases. Therefore, it is considered that the Mn^{3+} ions exist at $x = 0.00$ and the amount of Mn^{3+} decreases with x .

Figure 5 shows the IPFY XAS spectra of Mn $2p$. The peak around 640 eV corresponds to the transition from the Mn $2p_{3/2}$ core level to the Mn $3d e_g$ state and the peak around 643 eV corresponds to the transition from the Mn $2p_{3/2}$ core level to the Mn $3d t_{2g}$ state. The other peak around 653 eV corresponds to the Mn $2p_{1/2}$ edge. The sharp peak around 640 eV is specific for Mn^{4+} where the e_g orbitals are unoccupied. In addition, we observed a small peak between the peaks around 640 eV and 643 eV at $x = 0.00$. The small peak corresponds to the Mn $2p_{3/2}$ edge of Mn^{3+} , indicating that the $x = 0.00$ sample contains the Mn^{3+} ions at the bulk. The small peak vanished with increasing x , suggesting that the Mn^{3+} ions change into the Mn^{4+} ions as the ratio of Li increases up to $x = 0.05$.

The Ni $2p$ and Mn $2p$ XPS spectra, which are very

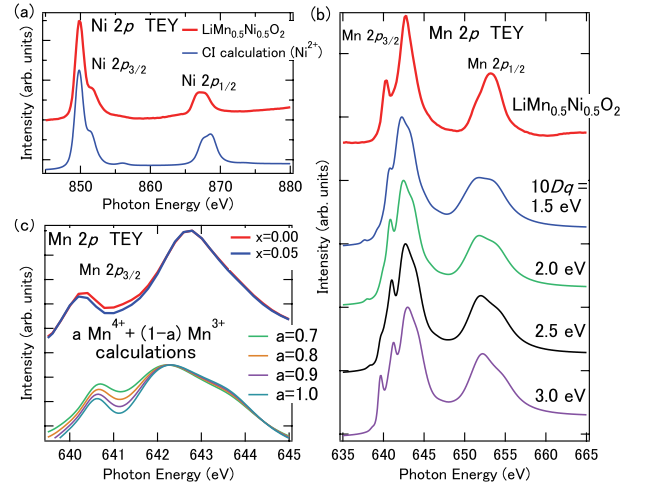


FIG. 4: (a) Calculated Ni $2p$ XAS spectrum (blue line) compared with the Ni $2p$ XPS of $LiMn_{0.5}Ni_{0.5}O_2$ (red line). (b) Calculated Mn $2p$ XAS spectra as a function of $10Dq$. The calculated results are compared with the Mn $2p$ XPS of $LiMn_{0.5}Ni_{0.5}O_2$ (red line). (c) Mn $2p$ XAS spectra of $Li_{1+x}[Mn_{0.5}Ni_{0.5}]_{1-x}O_2$ ($x = 0.00$ and 0.05) and their comparison with the theoretical spectra obtained by adding the calculated spectrum of Mn^{4+} and that of Mn^{3+} .

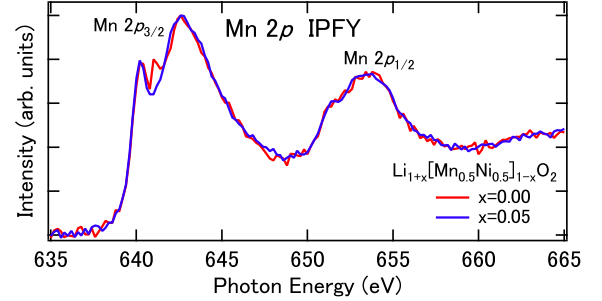


FIG. 5: IPFY Mn $2p$ XAS of $Li_{1+x}[Mn_{0.5}Ni_{0.5}]_{1-x}O_2$ ($x = 0.00$ and 0.05)

surface sensitive, indicate that the Ni and Mn valence states do not change at the surface between $x = 0.00$ and 0.05 in $Li_{1+x}[Mn_{0.5}Ni_{0.5}]_{1-x}O_2$. The small contribution of Mn^{3+} is suggested for $x = 0.00$ in the Mn $2p$ TEY XAS which is more bulk sensitive than the Mn $2p$ XPS. The most bulk sensitive IPFY XAS spectra indicate that the Jahn-Teller active Mn^{3+} component exists at $x = 0.00$ and is dramatically suppressed by increasing x . The existence of Mn^{3+} at $x = 0.00$ can be attributed to the site exchange between Ni and Li. The fact that the Mn^{3+} peak is removed with x indicates that the almost all the Mn^{3+} ions are changed to Mn^{4+} by introducing the excess Li up to $x = 0.05$ and probably by suppressing the site exchange. It is considered that the Jahn-Teller active Mn^{3+} ions at the bulk deteriorate the cycle performance of the Li ion battery. Therefore, the decrease

of Mn^{3+} or the decrease of the site exchange with x is useful to improve the performance.

The present work has been performed under the ap-

provals of the Photon Factory Program Advisory Committee (Proposal No. 2013G680).

-
- [1] K. Mizushima, P. C. Jones, P. J. Wiseman, and J. B. Goodenough, *Mater. Res. Bull.* **15**, 783 (1980).
 - [2] E. Plichta, S. Slane, M. Uchiyama, M. Salomon, D. Chua, W. B. Ebner, and H. W. Lin, *J. Electrochem. Soc.* **136**, 1865 (1989).
 - [3] H. F. Gibbard, *J. Power Sources* **26**, 81 (1989).
 - [4] T. Nagura and K. Tazawa, *Prog. Batteries Sol. Cells* **9**, 20 (1990).
 - [5] T. Ohzuku and Y. Makimura, *Chem. Lett.* **30**, 744 (2001).
 - [6] B. L. Cushing and J. B. Goodenough, *Solid State Science* **4**, 1487 (2002).
 - [7] Y. Idemoto, T. Hasegawa, N. Kitamura, and Y. Uchimoto, *Electrochemistry* **79**, 15 (2011).
 - [8] H. Wadati, D. G. Hawthorn, T. Z. Regier, G. Chen, T. Hitosugi, T. Mizokawa, A. Tanaka, and G. A. Sawatzky, *Appl. Phys. Lett.* **97**, 022106 (2010).
 - [9] H. Wadati, A. J. Achkar, D. G. Hawthorn, T. Z. Regier, M. P. Singh, K. D. Truong, P. Fournier, G. Chen, T. Mizokawa, and G. A. Sawatzky, *Appl. Phys. Lett.* **100**, 193906 (2012).
 - [10] F. M. F. de Groot, J. C. Fuggle, B. T. Tole, and G. A. Sawatzky, *Phys. Rev. B* **40**, 5715 (1990).
 - [11] M. Medarde, A. Fontaine, J. L. García-Muñoz, J. Rodríguez-Carvajal, M. de Santis, M. Sacchi, G. Rossi, and P. Lacorre, *Phys. Rev. B* **46**, 14975 (1992).
 - [12] A. N. Vasiliev, O. S. Volkova, L. S. Lobanovskii, I. O. Troyanchuk, Z. Hu, L. H. Tjeng, D. I. Khomskii, H.-J. Lin, C. T. Chen, N. Tristan, F. Kretschmar, R. Klingeler, and B. Büchner, *Phys. Rev. B* **77**, 104442 (2008).